Exploring the impact of whole-body vibration on bone metastasis and vascularization in a murine model of breast cancer

Breast cancer (BC) is the most prevalent cancer and primary cause of cancer-related fatalities among women worldwide, highlighting the urgency for effective interventions. Although advancements in early detection and treatment have enhanced survival rates, metastasis to distant organs, particularly bones, poses a significant challenge. Bone metastasis in BC often leads to osteolytic destruction, initiating a detrimental cycle of bone degradation and cancer progression. Despite patients with bone-only BC metastasis exhibit a more favorable prognosis than patients for whom metastasis is more extensive, the condition remains largely incurable, resulting in severe complications known as skeletal-related events. Current pharmacological interventions, such as bisphosphonates and denosumab, offer relief, but present long-term risks. Due to the mechanosensitivity of bone, exercise has been explored as a non-pharmacological approach; however, its applicability is hindered by the physical challenges faced by patients with BC. This study investigated whole-body vibration (WBV) as a potential passive exercise, demonstrating bone-anabolic responses without the risks associated with traditional exercise. Existing evidence supports WBV's efficacy in preserving bone health in various contexts, including childhood cancer survivors [1]. However, the specific effects on BC-induced bone loss remain unexplored. This study used mice with mammary tumors to assess the protective effects of WBV against metastatic BC-induced bone loss. In addition, this study examined the structure of the bone marrow vasculature in BC metastasis, considering its role in tumor progression and drug delivery. Employing synchrotron radiation-based computed tomography (SRCT, 2.74-μm cubic voxel) with vascular casting, our research aimed to provide valuable insights into the potential benefits of WBV in mitigating BC-induced bone loss and its impact on the associated bone marrow vasculature [2].

Eight-week-old female BALB/c mice were anesthetized, and 4T1 tumor cells were injected into the mammary fat pad. 4T1-bearing mice were assigned to two groups: those treated with Whole-Body Vibration (BC-WBV) and sham-treated controls (BC-Sham). Age-matched mice (intact) were sham-treated to assess the progression of bone loss induced by the 4T1 cell injection. The BC-WBV group experienced 20 min/day of vertical sine-wave vibration with a 0.3 g amplitude at 90 Hz for five days a week, concurrently with similar handling for BC-Sham and Intact mice, albeit without vibration exposure.

Three weeks after the onset of the vibration protocol, the mice were euthanized, and the right and left tibiae were harvested from the three groups for SRCT and H&E histology, whereas the subsets of BC-Sham and BC-WBV mice underwent vascular casting. Briefly, under isoflurane anesthesia, mice underwent laparotomy, followed by catheterization of the left ventricle and euthanization. The vascular bed was cast using a zirconium-based contrast agent (ZrCA), consisting of a mixture of agarose and colloidal ZrO_2 particles. The right tibia was then harvested and fixed in formalin.

The proximal metaphyseal portion of all specimens was scanned with a 17.95-keV X-ray at SPring-8 **BL20B2**. Calibration using K_2HPO_4 phantom solutions yielded the relation: $\mu = 7.58 \times BMD + 1.03$, where μ (cm^{-1}) is the linear absorption coefficient, proportional to the grayscale value of reconstructed bone image, and BMD (g/cm^3) is the bone mineral density. The vascular-cast specimens underwent additional scanning using an 18.05-keV X-ray, which enhanced the contrast of the blood vessels due to the sharp absorption jump of ZrCA. Therefore, selective visualization of vascular structures was possible by subtraction between a pair of 17.95- and 18.05-keV images [3]. Figure 1 shows the

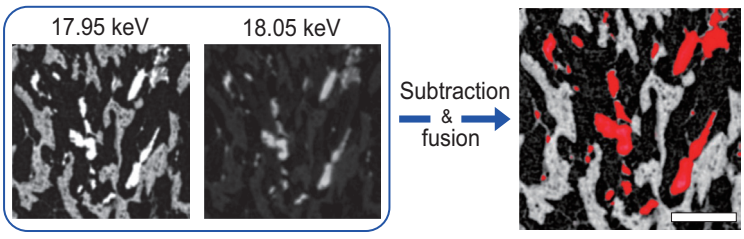

Fig. 1. Images reconstructed from scan data sets at 17.95 keV and 18.05 keV and their fusion via image subtraction, segmented into blood vessels (red) and trabecular bone (gray). Bar, 100 μm.

images of the tibial marrow region reconstructed from SRCT using 17.95- and 18.05-keV light and their fusion.

Histological H&E sections demonstrated metastatic lesions that extensively infiltrated the bone marrow cavity in both the BC-Sham and BC-WBV groups; however, a significant difference was found in the degree of bone destruction between the two groups. Figure 2 shows the cross-sectional bone reconstructions from the Intact, BC-Sham, and BC-WBV groups, and the bone structural indices and mean BMD of the three groups. Osteolytic bone deterioration in the BC-Sham group was characterized by a decrease in cortical bone thickness, trabecular bone volume fraction, trabecular bone thickness, trabecular number, and mean BMD in both the cortex and trabeculae. In contrast, no significant differences were found in bone features other than trabecular bone thickness between the BC-WBV and Intact groups, indicating the bone-protective effects of WBV.

Figure 3 shows three-dimensional reconstructions of the marrow vasculature and trabeculae, as well as the distribution of diameter-specific vascular volume fractions in BC-Sham and BC-WBV mice. On average, BC-WBV mice had smaller vessel diameters and spacing and a trend toward higher vessel numbers compared to BC-Sham mice. Furthermore, WBV shifted the distribution of diameter-specific vascular volume fractions toward smaller vessel diameters and decreased the heterogeneity of the marrow vessel diameter. Solid tumor vasculature is characterized by increased heterogeneity in vessel diameter, which causes not only low perfusion, but also heterogeneous perfusion, leading to regional tissue hypoxia. Hypoxia confers aggressive and metastatic phenotypes to tumors, and heterogeneous perfusion coupled with increased interstitial fluid pressure leads to inefficient delivery of antitumor drugs. Therefore, WBV may be effective against tumor growth and poor distribution of antitumor drugs [4].

In summary, WBV mitigates bone loss in BC bone metastasis, which may be partly due to the alteration of the marrow vasculature, which is favorable for reducing regional hypoxia in BC metastatic bone lesions. Further studies are needed to clarify the multiple actions of WBV on the bone, tumor, and marrow vasculature and how they contribute to bone protection in BC metastasis.

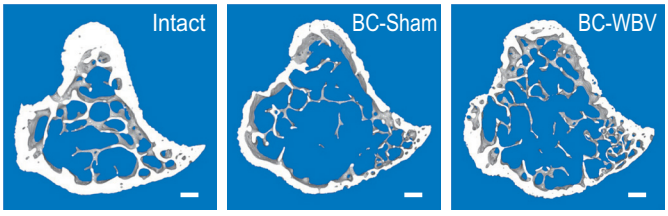

Bone structural indices and mineral density

	Intact (n = 5)	BC-Sham (n = 15)	BC-WBV (n = 13)
Cortical bone thickness (μm)	180.0 ± 4.0	99.8 ± 4.6##	117.2 ± 9.5*
Trabecular bone volume fraction (%)	6.82 ± 0.58	3.80 ± 0.46##	4.88 ± 0.55
Trabecular bone thickness (μm)	45.0 ± 0.8	33.3 ± 1.3#	33.5 ± 2.1#
Trabecular bone number density (mm^{-3})	1688 ± 272	1179 ± 195#	1575 ± 203*
Cortical bone mineral density (g/cm^3)	1.26 ± 0.03	1.13 ± 0.02##	1.18 ± 0.02**
Trabecular bone mineral density (g/cm^3)	1.01 ± 0.03	0.93 ± 0.01##	0.95 ± 0.01*

Data are presented as mean±SD. #P<0.05, ##P<0.01 *vs.* Intact; *P<0.05, **P<0.01 *vs.* BC-Sham.

Fig. 2. Reconstructions of proximal tibial diaphyseal bone from each of Intact, BC-Sham, and BC-WBV groups, binarized with a threshold of 0.5 g/cm^3 (top) and the summary of the bone structural indices and mineral density (bottom). Bar, 100 μm.

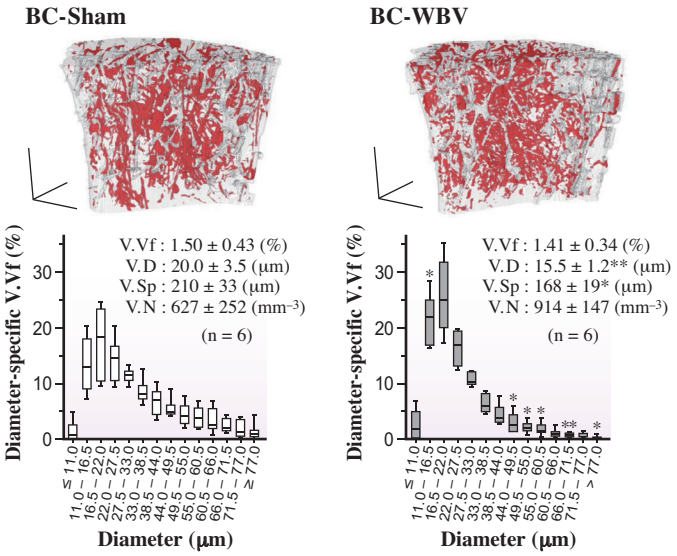

Fig. 3. Reconstructions of blood vessels and trabeculae (top) and boxplots of the diameter-specific vascular volume fraction (bottom) in the medullary region of proximal metaphyseal tibiae of BC-Sham and BC-WBV groups. V.Vf, vascular volume fractions; V.N, vessel number; V.Sp, vessel spacing; V.D, vessel diameter. The lengths of orthogonal line segments are all 0.5 mm. *P < 0.05, **P < 0.01 *vs.* BC-Sham.

Takeshi Matsumoto

Industrial and Social Sciences, Tokushima University

Email: t.matsumoto@tokushima-u.ac.jp

References

[1] R. J. Mogil *et al.*: JAMA Oncol. **2** (2016) 908.
[2] *T. Matsumoto and A. Mukohara: Calcif. Tissue Int.* ***111*** *(2022) 535.*
[3] T. Matsumoto *et al.*: Lab. Invest. **93** (2013) 1054.
[4] R. Lugano *et al.*: Cell Mol. Life Sci. **77** (2020) 1745.